Monthly Notices of the ROYAL ASTRONOMICAL SOCIETY
MNRAS **444,** 527–541 (2014) doi:10.1093/mnras/stu1450

From *Spitzer* Galaxy photometry to Tully–Fisher distances

J. G. Sorce,[1,2★] R. B. Tully,[3] H. M. Courtois,[1] T. H. Jarrett,[4] J. D. Neill[5] and E. J. Shaya[6]

[1]*Université Lyon 1, CNRS/IN2P3, Institut de Physique Nucléaire, F-69100 Lyon, France*
[2]*Leibniz-Institut für Astrophysik, D-14482 Potsdam, Germany*
[3]*Institute for Astronomy, University of Hawaii, 2680 Woodlawn Drive, HI 96822, USA*
[4]*University of Cape Town, Private Bag X3, Rondebosch 7701, Republic of South Africa*
[5]*California Institute of Technology, 1200 E. California Blvd MC 278-17, Pasadena, CA 91125, USA*
[6]*Department of Astronomy, University of Maryland, College Park, MD 20742, USA*

Accepted 2014 July 17. Received 2014 July 17; in original form 2014 June 19

ABSTRACT

This paper involves a data release of the observational campaign: *Cosmicflows with Spitzer* (CFS). Surface photometry of the 1270 galaxies constituting the survey is presented. An additional ∼400 galaxies from various other *Spitzer* surveys are also analysed. CFS complements the *Spitzer Survey of Stellar Structure in Galaxies*, that provides photometry for an additional 2352 galaxies, by extending observations to low galactic latitudes ($|b| < 30°$). Among these galaxies are calibrators, selected in the *K* band, of the Tully–Fisher relation. The addition of new calibrators demonstrates the robustness of the previously released calibration. Our estimate of the Hubble constant using supernova host galaxies is unchanged, $H_0 = 75.2 \pm 3.3$ km s^{-1} Mpc^{-1}. Distance-derived radial peculiar velocities, for the 1935 galaxies with all the available parameters, will be incorporated into a new data release of the Cosmicflows project. The size of the previous catalogue will be increased by 20 per cent, including spatial regions close to the Zone of Avoidance.

Key words: galaxies: photometry – distance scale – infrared: galaxies.

1 INTRODUCTION

Cosmicflows (Courtois & Tully 2012a,b; Tully & Courtois 2012; Tully et al. 2013) is a project to map radial peculiar velocities of galaxies within 200 Mpc with the ultimate goal of reconstructing and simulating the motions of the large-scale structures and explaining the deviation of our Galaxy from the Hubble expansion of 630 km s^{-1} (Fixsen et al. 1996). Radial peculiar velocities, $v_{\rm pec}$, are obtained from the redshift and an independent luminosity distance measurement, $v_{\rm pec} = v_{\rm mod} - H_0$ d, where H_0 is the Hubble constant and $v_{\rm mod}$ is the velocity with respect to the cosmic microwave background with a minor correction for cosmological effects (Tully et al. 2013). Distances in the project *Cosmicflows* are mainly obtained with the luminosity–linewidth rotation rate correlation or Tully–Fisher relation (TFR; Tully & Fisher 1977), a distance estimator which provides coverage up to 200 Mpc. The TFR necessitates two very accurate observations of a galaxy to compute its distance – an H I profile and a photometric measurement. Observations in the radio domain to obtain rotation rates of galaxies have made great advances in the past few years and more than 10 000 adequate linewidths of galaxies are available (Courtois et al. 2011a) in the Extragalactic Distance Database[1] (EDD; Courtois et al. 2009; Tully et al. 2009). The *Cosmicflows with Spitzer* (CFS) programme, combined with an additional sample of galaxies from various *Spitzer* programmes, uses the space-based *Spitzer* telescope (Werner et al. 2004) to address the photometric requirement of the project *Cosmicflows*.

In this paper, we present the reduction of wide-field images of 1270 galaxies observed with the 3.6 μm channel of the InfraRed Array Camera (IRAC; Fazio et al. 2004) on board the *Spitzer* Space Telescope during its post-cryogenic period, cycle 8. This survey complements four other large *Spitzer* surveys, the *Spitzer* Infrared Nearby Galaxy Survey (SINGS; Muñoz-Mateos et al. 2009), the Local Volume Legacy Survey (LVL; Dale et al. 2009) led during the cryogenic phase of the *Spitzer* mission, the Carnegie Hubble Program (CHP; Freedman et al. 2011) and the *Spitzer* Survey of Stellar Structure in Galaxies (S^{4}G; Sheth et al. 2010) obtained in the post-cryogenic period. From these surveys and several other small programmes, approximately 1000 additional galaxies are of interest to the *Cosmicflows* project. Approximately 35 per cent of

★ E-mail: j.sorce@ipnl.in2p3.fr

[1] http://edd.ifa.hawaii.edu/

these galaxies are reduced using the *Spitzer*-adapted version of ARCHANGEL while S^{4}G-pipeline (Munõz-Mateos et al., in preparation) supplies the rest of it. With the availability of such a large number of photometric measurements, the robustness of both the TFR calibration method and the TFR at 3.6 μm can be confirmed.

In the subsequent section, we describe the complete photometric sample, then we present the observation-reduction process applied to CFS and approximately 400 supplementary galaxies and the results. In the third section, the mid-IR TFR (Sorce et al. 2013, although at that time considered preliminary) is shown to be robust. The associated Hubble constant estimate is confirmed in the fourth section. In the last section, we derive accurate distance estimates for 1935 galaxies with acceptable inclinations and available linewidths that either we have reduced or that come from the S^{4}G analysis.

2 OBSERVATIONAL SAMPLES

In Fig. 1, the 1270 galaxies of the CFS survey are distinguished by their occurrence in five subsamples: (1) the TF calibrators (Calib), (2) the hosts of SNIa sample (SNIa-H), (3) the V3k, 3000 km s^{-1} sample (V3k), (4) the *IRAS* point source redshift sample (PSCz) and (5) the flat galaxy sample (FG). These subsamples are completed with galaxies from various surveys. If a galaxy lies within multiple samples, in the following the galaxy is assigned to the sample that includes it that is discussed first. Galaxies of interest to the project but which do not fall into one of the previous categories constitute the sixth subsample. All these supplementary galaxies are mostly from S^{4}G (65 per cent). Among the ∼ 400 galaxies left, most galaxies have been observed by SINGS (2 per cent), LVL (3 per cent) and CHP (16 per cent) programmes.

(i) The first two of these subsamples have already been described (Tully & Pierce 2000; Tully & Courtois 2012; Courtois & Tully 2012b) and partly used at 3.6 μm to calibrate the TFR in the mid-infrared (Sorce et al. 2013) and to define an absolute zero-point to the SNIa scale (Sorce, Tully & Courtois 2012b), respectively. Approximately one-third of the first subsample is constituted of galaxies observed for CFS. Others have been observed by previous *Spitzer* programmes, mostly CHP and S^{4}G. Half of the SNIa subsample is made of CFS observations while the other half contains mostly CHP observations.

(ii) The third subsample is a catalogue developed over the years called V3k (Tully et al. 2008). It extends up to the velocity limit, 3000 km s^{-1}, imposed by the capabilities of early-generation radio telescopes to obtain usable H I profiles and gives coverage of the traditional Local Supercluster (de Vaucouleurs 1953). Fig. 1 and the top panel of Fig. 2 show that the majority of these galaxies are of types later than Sa. Types come from the HyperLeda data base (Paturel et al. 2003). Fig. 2 bottom confirms that the heliocentric velocities of these galaxies are $V_h < 3300$ km s^{-1} with heliocentric velocities coming from EDD. Among the 683 galaxies available for this third subsample about a quarter comes from the CFS survey. This sample provides a high density of the Local Supercluster centred on Virgo.

(iii) The next subsample is based on the redshift survey PSCz (Saunders et al. 2000) of sources drawn from a flux-limited sample at 100 μm obtained with the *InfraRed Astronomical Satellite* (*IRAS*). The sample is dominated by normal spirals distributed around the Sc type as Figs 1 and 2 show. The heliocentric velocity limit is 6000 km s^{-1} to obtain reasonable H I lines with current radio telescopes. This subsample includes the Norma–Hydra–Centaurus and the Perseus–Pisces superclusters in the opposite directions and many low-latitude galaxies – offering good coverage above $|b| = 5°$. The bifurcation between our flow direction and a motion towards Perseus–Pisces highlighted by Erdoğdu et al. (2006) will be located thanks to this subsample. The PSCz sample will also strongly constrain the CMB dipole component within 6000 km s^{-1}. CFS contains the majority (445) of these galaxies.

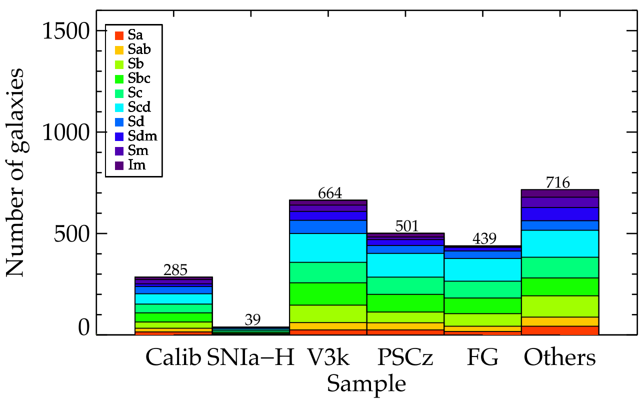

Figure 1. Histogram of the number of galaxies per subsamples in CFS and diverse programmes, mostly S^{4}G (65 per cent). Calib is constituted of TFR calibrators, SNIa-H contains hosts of SNIa, V3k is built of galaxies with $v_{hel} < 3000$ km s^{-1}, PSCz is derived from the *IRAS* point source redshift survey and FG is a catalogue of flat galaxies. 'Others' stands for galaxies of interests which do not fall into one of the previously cited categories. The gradient of colours shows the proportion of each morphological type from the HyperLeda Database in each sample.

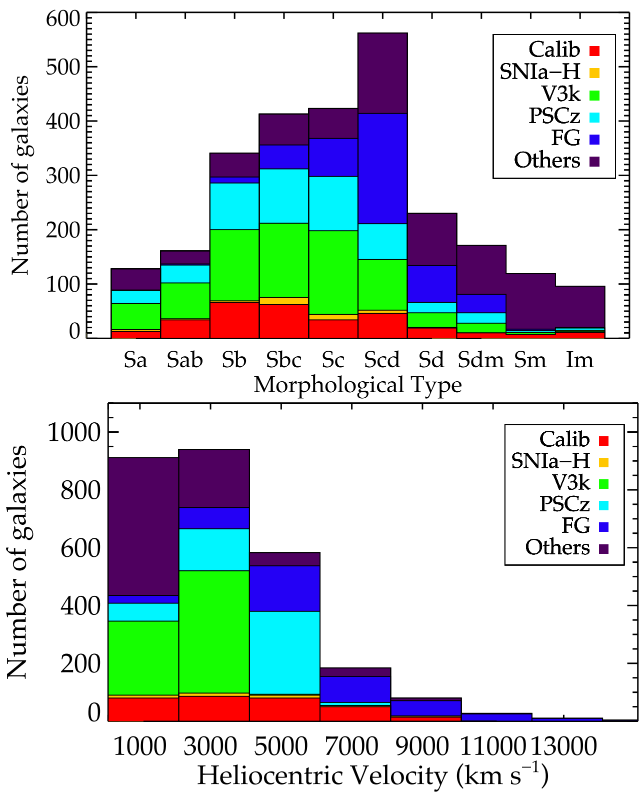

Figure 2. Histograms of the morphological type (top) from HyperLeda and of the heliocentric velocity (bottom) from EDD for the whole compilation of galaxies. The gradient of colours gives in which proportion each subsample contribute to a given type (top) and range of heliocentric velocities (bottom).

(iv) The last subsample is constituted of flat galaxies from the catalogue of Karachentsev et al. (1999). These edge-on systems have a major to minor axis ratio greater than 7 implying minimal de-projection of their H I linewidths. The flat galaxies are principally of type Scd, as shown in Figs 1 and 2 (top panel). They constitute a homogeneous class of H I-rich systems but they have a low space density partly because of the strong inclination constraint. Extinction problems existing at optical bands and for ground-based telescoped are practically removed with IRAC 3.6 μm. The entire flat galaxy subsample comes from CFS observations.

Fig. 3 illustrates the combined coverage of CFS and other relevant surveys with *Spitzer* Space Telescope. CFS gives special attention to galaxies at low galactic latitudes for two reasons. First, CFS complements the important S^4G survey that has a $|b| = 30°$ lower limit and that supplies most of the other galaxies. Secondly, we recognize that photometry from *WISE*, the *Wide-Field Infrared Survey Explorer* (Wright et al. 2010), will be useful but be at a competitive disadvantage to *Spitzer* in the crowded star fields at lower galactic latitudes because of resolution issues. As a result, future catalogues of the Cosmicflows project will contain more data close to the Zone of Avoidance than the second catalogue (CF2) of the project superimposed on the same figure.

In Section 3, a comparison between 241 mag from S^4G-pipeline and from the *Spitzer*-adapted version of ARCHANGEL used in this paper reveals the very good agreement between both magnitudes. As a result, S^4G-magnitudes are directly used to derive distances for the relevant galaxies in the last section. In the next section, we focus mostly on the CFS sample although the additional *Spitzer* archival galaxies minus S^4G's are processed equally.

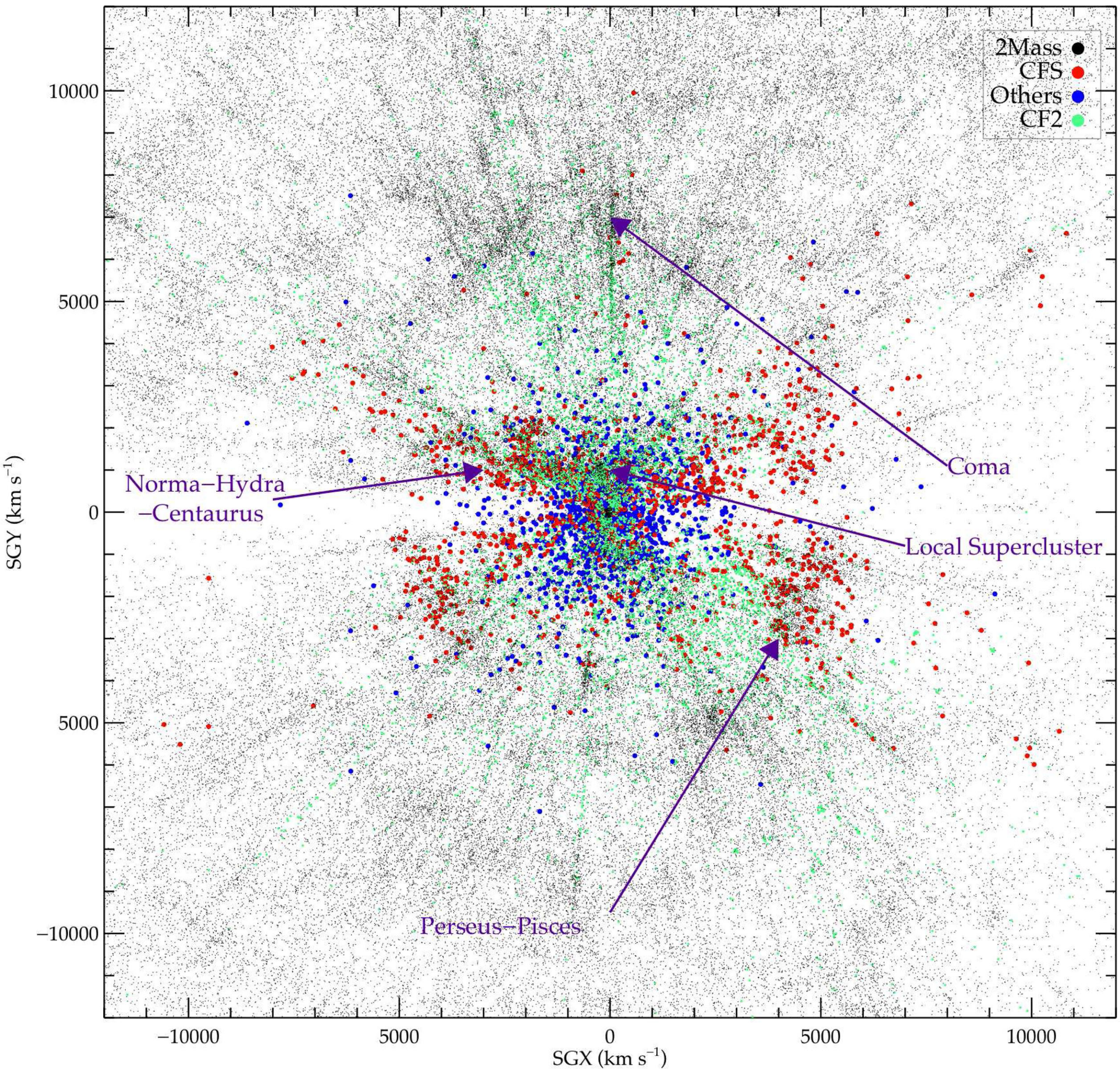

Figure 3. In the XY supergalactic plane, galaxies of the CFS survey (red dots) are superimposed on the 2MASS redshift catalogue (tiny black dots). Blue dots stand for galaxies of interests to the *Cosmicflows* project but observed by different programmes, mostly S^4G. A few superclusters are identified by violet arrows. CFS completes previous surveys with galaxies at low galactic latitudes. Green dots represents the second catalogue of the Cosmicflows project. Future catalogues of the Cosmicflows project will have a better coverage near the Zone of Avoidance, reconstructions of the Local Universe will be more accurate in that region.

3 REDUCTIONS, ANALYSES AND COMPARISONS

3.1 Reductions

The post-basic calibrated data of the 1270 observed galaxies for the CFS programme are available at the Spitzer Heritage Archive. Every galaxy has been observed with the first channel of the IRAC instrument where a point spread function with a FWHM 1.66 arcsec is sampled with 1.2 arcsec pixels. The field of view is 5.2 × 5.2 arcmin^2 which is adequate to include most galaxies beyond twice their diameter at the 25th isophote (mag arcsec^{-2}) in the *B* band. Consequently, except for a few cases, galaxies (1219 out of 1270) have been mapped within a single field exposed during four minutes (the total duration of one observation is 8.6 min), 45 have been mapped with four fields, five with nine fields and one, PGC62836 (NGC 6744), with 16 fields. Every resulting composite field extends to 8.5 exponential scalelengths ensuring that 99 per cent of the light of the galaxy is captured. The galaxies have inclination $i > 45°$ and are not perturbed by – or confused with – a second object in the H I beam ensuring that the TFR can be applied to them later on with minimized uncertainties.

The photometry is carried out with a *Spitzer*-adapted version of ARCHANGEL (Schombert 2007; Schombert & Smith 2012) described in detail in Sorce, Courtois & Tully (2012a). Briefly, ARCHANGEL performs the masking of stars and flaws and it replaces masked regions by mean isophote values. It fits ellipses to isophotes with increasing radii. It compresses the 2D information into unidimensional surface brightness and magnitude growth curves. Finally, parameters such as extrapolated magnitudes are derived. We run ARCHANGEL twice on each galaxy. The first run supplies the second run with parameters to improve the results. In the second run, we force the ellipse fitting up to at least $1.5 \times a_{26.5}$ – radius of the 26.5 mag arcsec^{-2} isophote at 3.6 μm – to ensure that 99 per cent of a galaxy light is captured. Position angles and ellipticities are frozen only at large radii – basically a_{24}, radius of the 24 mag arcsec^{-2} isophote at 3.6 μm – where the noise dominates, except when a simple visualisation shows that a smaller freezing radius is required. Very flat galaxies are mostly among the exceptions where the masking fails without a smaller freezing radius: the edges are inevitably masked if ellipses are not frozen at small radii. In any case, position angles and ellipticities at medium radii overall do not affect magnitudes, the most important parameter for the TFR. Sorce et al. (2012a) showed that the major contribution to the magnitude uncertainties is the sky setting. Every source of uncertainty included, the total magnitude uncertainty is still held below 0.04 mag (0.05 with extinction, aperture and *k*-corrections) for normal spiral galaxies.

For each galaxy, we derive the major axis radius in arcsec of the isophote at 26.5 mag arcsec^{-2} in the [3.6] band, $a_{26.5}$, and of the annuli enclosing respectively 80, 50 and 20 per cent of the total light, a_{80}, a_e and a_{20} (the subscript 'e' stands for 'effective' – a common terminology). We compute also the corresponding surface brightnesses μ_{80}, μ_e and the average $\langle\mu_e\rangle$ of the surface brightnesses between 0 and 50 per cent of the light, μ_{20} and the average $\langle\mu_{20}\rangle$ between 0 and 20 per cent of the light, in mag arcsec^{-2}. The central disc surface brightness in mag arcsec^{-2}, μ_0, the exponential disc scalelength in arcsec, α, the mean *b*/*a* ratio and its variance, the position angle and the concentration index a_{80}/a_{20} are also given. Three magnitudes are calculated: the magnitude at the 26.5th isophote, $[3.6]_{26.5}$, the total magnitude obtained from the extrapolation of the growth curve, $[3.6]_{tot}$ (the uncertainty on the rational function fit used to derive $[3.6]_{tot}$ is also given) and the extrapolated magnitude assuming a continuous exponential disc, $[3.6]_{ext}$. All the magnitudes are given in the AB system. We recommend to use $[3.6]_{ext}$ even if the three magnitudes are very similar.

Isophotes, surface brightness profiles and growth curves are available for the 1270 galaxies on line along with a table of the derived parameters at the EDD website. These plots are also available in EDD for the additional ∼400 galaxies from other programmes drawn from the Spitzer archive.

3.2 Analyses

In this subsection, we present the different parameters derived with the software ARCHANGEL for each one of the CFS galaxies. We claim at the beginning of Section 3 that we choose to observe each galaxy to within at least twice d_{25} to capture most of galaxy lights and to minimize magnitude measurement uncertainties. Then, we force ellipse fitting up to $1.5 \times a_{26.5}$. Fig. 4 confirms that d_{25} from RC3 used to set observations and $a_{26.5}$ obtained after reduction are comparable representatives of size. The scatter is only 41 arcsec around a 1:1 linear relation. The observational sensitivity is sufficient for our ultimate goal since at 26.5 mag arcsec^{-2} the isophotal magnitudes are already very close to extrapolated ones as shown by Sorce et al. (2012a) and Fig. 5.

In the adapted version of ARCHANGEL the computation of the minor to major axis, *b*/*a*, ratio, is specifically defined as the mean of the *b*/*a* ratios between 50 and 80 per cent of the light. Measuring *b*/*a* ratios is not an easy task and a comparison with the ratios used in the Cosmicflows programme on Fig. 6 top shows that at least one *b*/*a* source cannot be trusted. Each value needs to be checked before any usage. Retained *b*/*a* values are from the *I*-band programme of Cosmicflows (Tully et al. 2013) and from HyperLeda if it comes from Paturel et al. (2003). Position angles on the other hand are in good agreements at the bottom of the same figure.

Histograms of the other parameters are given in Fig. 7 in mag arcsec^{-2} for surface brightnesses and in arcsec for corresponding

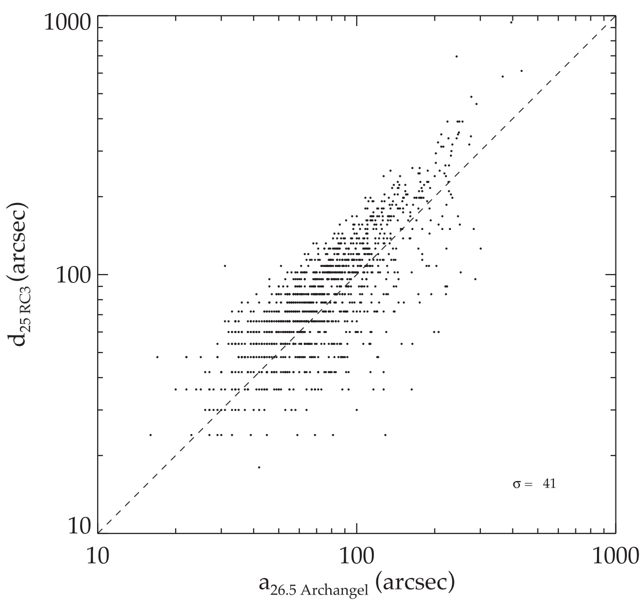

Figure 4. Comparison between the radius in arcsec of the isophote at 26.5 mag arcsec^{-2} in the [3.6] band obtained after reduction with ARCHANGEL and the radius at 25 mag arcsec^{-2} at the *B* band used beforehand to set observational parameters. These parameters are proportional to each other. In the case of an optimal 1:1 linear relation, the scatter is only 41 arcsec.

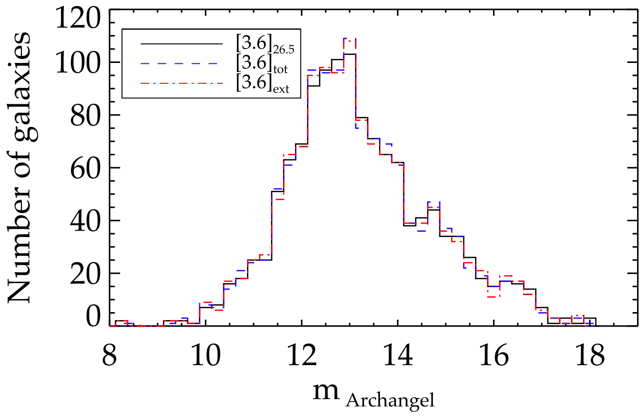

Figure 5. Histograms of the three magnitudes derived with ARCHANGEL. The magnitude at the 26.5 mag arcsec^{-2} isophote at 3.6 μm, $[3.6]_{26.5}$ (black straight line), the magnitude obtained by the extrapolation of the growth curve, $[3.6]_{\rm tot}$ (blue dashed line) and the magnitude assuming a continuous exponential disc, $[3.6]_{\rm ext}$ (red dot–dashed line).

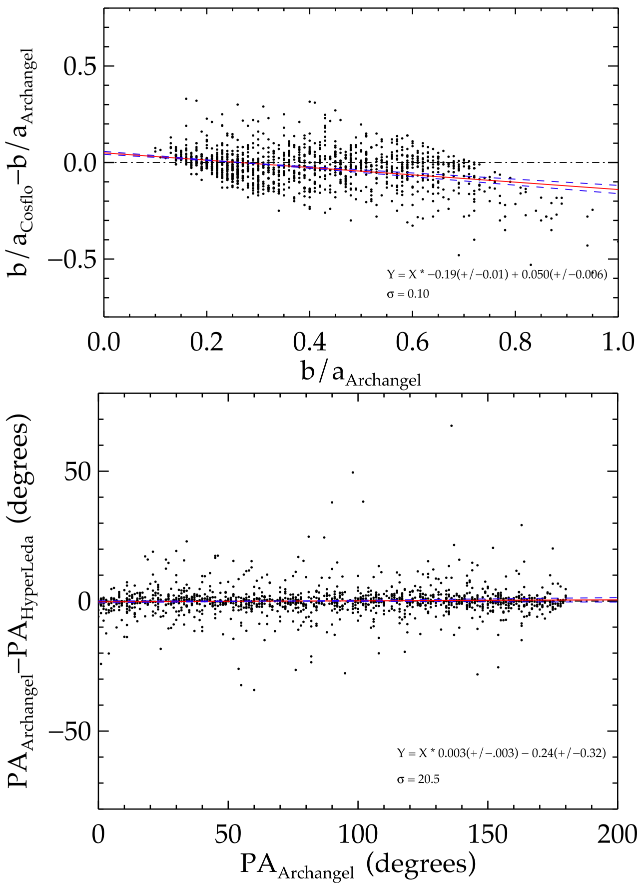

Figure 6. ARCHANGEL-derived *b*/*a* ratios (top) and position angles (bottom) versus Cosmicflows' minus ARCHANGEL's and Hyperleda's minus ARCHANGEL's. The black dot–dashed lines show the perfect cases $y = 0$, the red straight lines are linear fits to the data [with a 3σ clipping (20 galaxies) in the bottom panel], the blue dashed lines are the 1σ uncertainties.

radii. For all these parameters there is no outliers. It is worth noting that [3.6] μm surface brightnesses are overall below 24 mag arcsec^{-2} which is better than most optical surveys (about 26–28 mag arcsec^{-2} in the *B* band for example). IRAC is an exquisite imager for flatness and depth.

3.3 Comparisons

This last subsection demonstrates the agreement between magnitudes obtained with the *Spitzer*-adapted version of ARCHANGEL used in this paper and with alternative pipelines. Fig. 9 of Sorce et al. (2012a) had already revealed that ARCHANGEL and the software developed for the *GALEX* Large Galaxy Atlas (Seibert et al., in preparation) by the CHP team give relatively close magnitudes. Fig. 8 proves that this adapted version of ARCHANGEL computes magnitudes equally similar to the pipeline of the S^{4}G team. There is a slight tendency for S^{4}G values to be brighter for the largest galaxies. A cause can be the difference in masking. Another cause can be the sky setting that with S4G is done quite differently. Instead of using sky boxes, S^{4}G pipeline derives sky values out of annuli located just at the extremity of what they estimate to contain the totality of the galaxy light. This different sky setting might also explain the slight increase in the root mean square scatter (four galaxies rejected) which reaches ±0.1 instead of a scatter of 0.05 in the comparison between CHP and ARCHANGEL magnitude values. Attributed equally, the 0.1 scatter gives an uncertainty about ±0.07 mag for each source. Regardless, it is reassuring that our magnitudes are in agreements with these two alternative computations.

As a result, these three magnitudes can be used nearly interchangeably. For a better precision, they are averaged when more than one of them is available in the next sections.

4 ROBUSTNESS OF THE CALIBRATION OF THE MID-IR TFR

In this section, the robustness of both the calibration method and the mid-IR TFR (Sorce et al. 2013, hereafter S13) is shown. The 2013 calibration which was presented as preliminary, especially because of the lack of completeness of the calibrator sample, is confirmed. Magnitudes used in this section come from ARCHANGEL combined with an S^{4}G-pipeline or a CHP-pipeline magnitude or both when they are available. These raw magnitudes [3.6] are then corrected $[3.6]^{b,i,k,a}$ for (1) extinctions (both galactic and internal) $[3.6]^{b,i}$, (2) shift in fluxes due to Doppler effect $[3.6]^{k}$, and (3) extended emission from the point spread function outer wings and from scattered diffuse emission across the IRAC focal plane $[3.6]^{a}$. These corrections are described separately in (1) Cardelli, Clayton & Mathis (1989), Schlegel, Finkbeiner & Davis (1998), Giovanelli et al. (1995, 1997) and Tully et al. (1998), (2) Oke & Sandage (1968), Huang et al. (2007) and (3) Reach et al. (2005) and specifically for *Spitzer* IRAC 3.6 μm data in Sorce et al. (2012a). The resulting magnitudes are called $[3.6]^{b,i,k,a}$ in the rest of the paper where each superscript stands for a correction.

4.1 An updated list of galaxies

S13 derived a template TFR using 213 galaxies in 13 clusters. The zero-point calibration was given by 26 additional galaxies. The inverse fit was used to calculate the slope of the relation and a very small correction was computed to remove a bias. In this paper, the same analysis is done using an updated sample of template and zero-point calibrators. This sample is improved in two aspects. The number of calibrators is increased from 213+26 to 287+32. Also galaxies are now selected in the *K*-band which decreases the selection bias. The selection of calibrators is extended to be complete to $K = 11.75$ mag, the limit of the 2MRS 11.75 survey (Huchra et al. 2012). This new set of calibrators follows the same rules as in S13: (1) candidates are chosen out of a projection-velocity window,

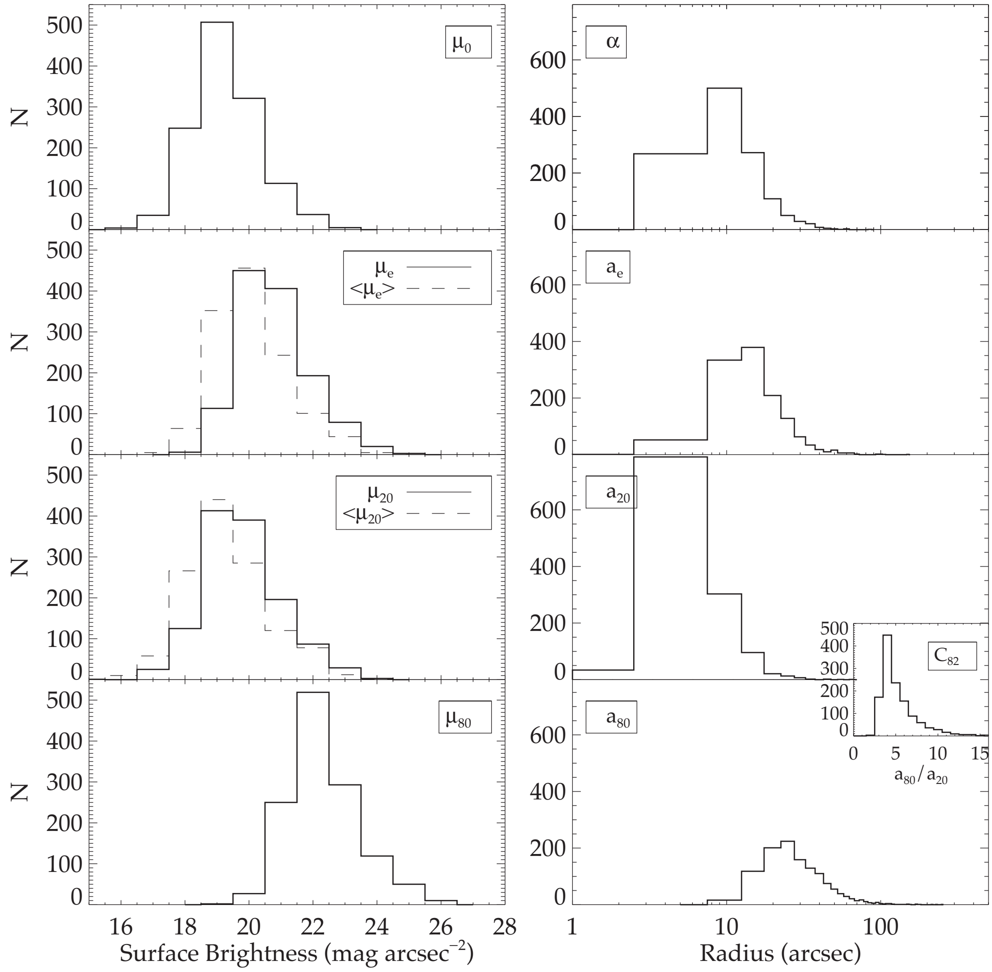

Figure 7. Histograms of some of the parameters computed with the ARCHANGEL software. Left, from top to bottom, histograms in solid lines of the central disc surface brightness μ_0 and of the surface brightnesses at 50, 20 and 80 per cent of the total light μ_e, μ_{20} and μ_{80} (mag arcsec^{-2}). Histograms of the average of the surface brightnesses between 0, 50 and 20 per cent of the light, $\langle\mu_e\rangle$ and $\langle\mu_{20}\rangle$ respectively, are overplotted in dashed lines. Right, from top to bottom, disc scalelength α and annuli encompassing 50, 20 and 80 per cent of the light a_e, a_{20} and a_{80}, in arcsec. The histogram of the concentration index, $C_{82} = a_{80}/a_{20}$ is overplotted in a small panel on the right-hand side of the a_{20} and a_{80} histograms.

(2) morphological types earlier than Sa are excluded, (3) H I profiles are not confused, (4) the candidates do not appear pathological, for example, exhibiting tidal disruption and (5) inclinations must be greater than 45°. The zero-point calibrators also need to have a very well known distance from Cepheid or Tip of the red giant branch measurements. There is no evidence that rejected galaxies preferentially lie in any particular part of the Tully–Fisher (TF) diagram (Tully & Courtois 2012).

H I linewidths are provided by the H I subproject of *Cosmicflows* (EDD website;[2] Courtois et al. 2009, 2011a), Table 1 (complete table online) gives the measurements for the calibrators. We proceed exactly as in S13:

(1) An inverse TFR is fitted to each one of the clusters separately. Fig. 9 top shows the example of the Virgo Cluster. Parameters for every cluster are given in Table 2. The inverse fit assumes errors only in linewidth to obtain results close to free of Malmquist magnitude selection bias. Yet, there will be a tiny bias residual because of the bright end cutoff of the luminosity Schechter function although it should be somewhat smaller than with the S13 calibration where, in addition, the selection was made in the *B* band. We investigate this bias relic at the end of this section.

(2) Because slopes are quite similar between clusters in Table 2, individual fits are consistent with the postulate of a universal TFR. Thus, the 13 clusters are combined into one template cluster. Virgo is taken as the reference cluster and each one of the 12 other clusters is shifted to be on the same scale. Three by three, clusters are inserted into the template and offsets between them and Virgo are found by an iterative process which relies on least-squares fit of the inverse TFR. Convergence is quick. We obtain a slope of -9.77 ± 0.19, insignificantly different from the previous slope -9.74 confirming the robustness of the S13 calibration and of the method. The universal slope and the offsets with respect to Virgo are shown on Fig. 9 bottom.

(3) The zero-point scale of the Cepheid calibrators is set by the distance modulus of the Large Magellanic Cloud, 18.48 ± [0.04–0.07] (Riess et al. 2011; Monson et al. 2012). Then, the 32 zero-point calibrators give the zero-point of the universal TFR assuming the slope of the cluster template. Their correlation is visible in the top panel of Fig. 10 where now absolute magnitudes replace apparent magnitudes. The zero-point of the TFR is the difference between the zero-point given by zero-point calibrators on Fig. 10 top and by

[2] http://edd.ifa.hawaii.edu; catalogue 'All Digital HI'.

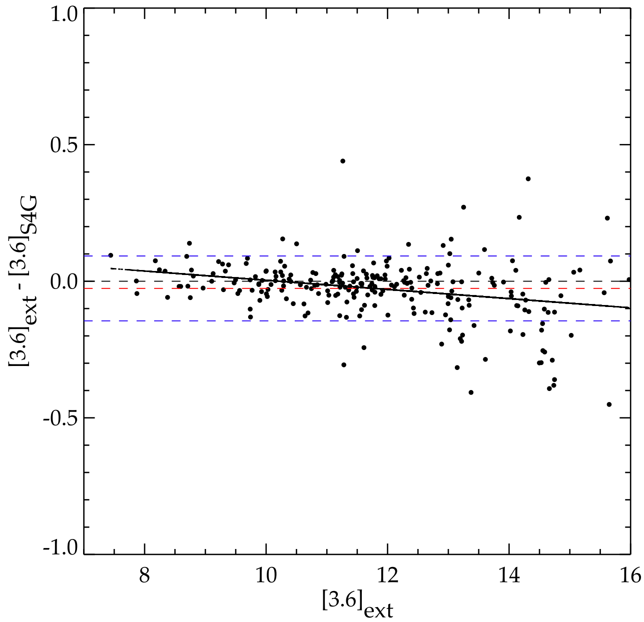

Figure 8. Comparisons between 241 [3.6] extrapolated ARCHANGEL and [3.6] S[4]G magnitudes. The fit at 3σ clipping (four galaxies rejected) has a slope of -0.02 ± 0.004 and a zero-point of 0.17 $\pm$0.04. The red dashed thick line stands for the offset at -0.02 mag and the blue dashed lines represent the scatter at 0.1 mag. Deviant cases except for two are low surface brightness galaxies, and we find no reason to reject ARCHANGEL values.

Virgo in Fig. 9 top: -20.31 ± 0.09. The zero-point is once again insignificantly larger than that of the S13 calibration of -20.34.

The universal relation at 3.6 μm is visible on Fig. 10 and is given by a slightly updated version of the S13 calibration:

$$M_{[3.6]}^{b,i,k,a} = -(20.31 \pm 0.09) - (9.77 \pm 0.19)(\log W_{mx}^{i} - 2.5) \quad (1)$$

with a scatter of 0.54 for the 13 clusters and 0.45 for the 32 zero-point calibrators. S13 already discussed the causes of such a scatter. Among these reasons, they evoke a colour term due to the fact that faster rotators tend to be redder and rise more quickly than bluer galaxies in the TF diagram (e.g. S13, their fig. 6). Following the earlier work, we apply a colour correction in the next subsection to confirm the colour-corrected TFR derived in S13.

4.2 The colour correction

Because of the increased number of data, we double check the colour term deriving a new estimate. The straight line fit given in Fig. 11 top is a least-squares minimization with respect to the difference in magnitude of a galaxy from the derived TFR. In the [3.6] band, a galaxy is offset from the TFR by

$$\begin{aligned}\Delta M_{[3.6]}^{\rm color} &= M^{b,i,k,a} + 20.31 + 9.77(\log W_{mx}^{i} - 2.5)\\ &= -(0.52 \pm 0.10)[(I^{b,i,k} - [3.6]^{b,i,k,a}) + 0.73]. \quad (2)\end{aligned}$$

Note that *I*-band magnitudes have been converted from the Vega to the AB system by making a 0.342 mag shift. Slope and zero-point are slightly smaller than those given in S13 (-0.47 and -0.36) but within the uncertainty. Still, for completeness, we use this new estimate. Colour adjusted parameters, $C_{[3.6]} = [3.6]^{b,\,i,\,k,\,a} - \Delta[3.6]^{\rm color}$, are derived accordingly and then, considered as pseudo-magnitudes to produce the colour-corrected calibration, proof of the robustness of the S13 calibration. The procedure described in the previous subsection is reiterated with a number of galaxies slightly decreased due to a lack of *I*-band measurements (273+31).

The colour-corrected calibration is visible on Fig. 11 bottom and given by

$$M_{C_{[3.6]}} = -(20.31 \pm 0.07) - (9.10 \pm 0.21)(\log W_{mx}^{i} - 2.5) \quad (3)$$

with 0.45 and 0.37 as new scatters. A summary of the derived parameters for the TFR in this paper are given in Table 2 as well as in Table 3 along those of S13 and those of Tully & Courtois (2012) for the *I* band. Although a direct comparison has some imprecision because of the different galaxy samples, the agreement is excellent.

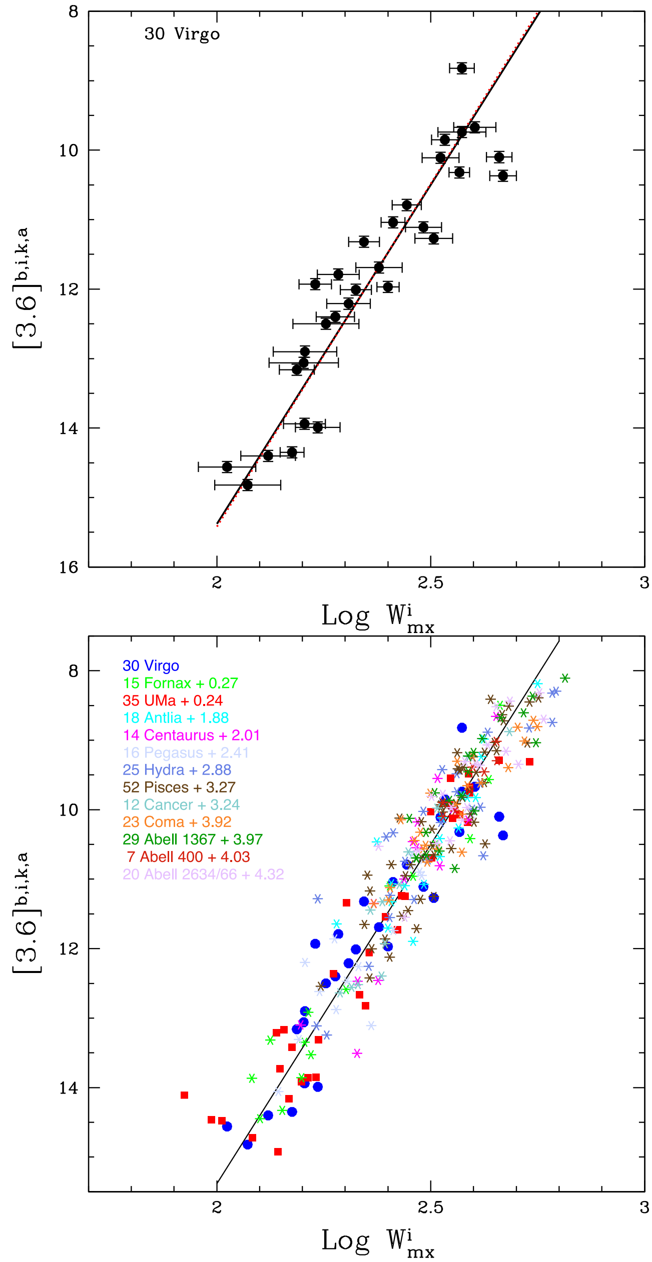

Figure 9. Top: inverse TFR at 3.6 μm for the Virgo Cluster in dotted red line. The solid black line stands for the inverse TF of the template cluster. Bottom: Universal inverse TFR at 3.6 μm obtained with 287 galaxies in 13 clusters. Numbers of galaxies selected for the calibration per clusters are given in front of clusters' names while distance modulus differences between each cluster and Virgo are visible after clusters' names.

Table 1. Calibrator parameters for the TFR (complete table online): (1) PGC number, (2) common name, (3) *I*-band-corrected magnitude, mag, (4) [3.6]-averaged corrected magnitude, mag, (5) pseudo-[3.6] magnitude, mag, (6) axial ratio, (7) inclination, degrees, (8) linewidth not corrected for inclination, km s^{-1}, (9) linewidth corrected for inclination, km s^{-1}, (10) logarithm of the inclination-corrected linewidth, (11) sample (ZP zero-point calibrators).

PGC	Name	$I^{b,i,k}_{\rm ext}$	$[3.6]^{b,i,k,a}_{\rm ave}$	$C^{b,i,k,a}_{[3.6]_{\rm ave}}$	b/a	Inc	W_{mx}	W^i_{mx}	W^i_{mxl}	Sample
2758	NGC 0247	7.79	9.10	8.98	0.31	76.	190	196	2.292	ZP
3238	NGC 0300	7.28	8.40	8.38	0.71	46.	140	195	2.290	ZP
9332	NGC 0925	8.96	10.25	10.14	0.57	57.	194	231	2.364	ZP
13179	NGC 1365	8.09	8.77	8.97	0.61	54.	371	459	2.662	ZP
13602	NGC 1425	9.50	10.72	10.64	0.46	65.	354	391	2.592	ZP
17819	NGC 2090	9.33	10.38	10.39	0.43	67.	277	301	2.478	ZP
21396	NGC 2403	7.11	8.46	8.32	0.53	60.	226	261	2.417	ZP
23110	NGC 2541	10.76	12.06	11.94	0.49	63.	188	211	2.325	ZP
26512	NGC 2841	7.53	8.65	8.63	0.45	66.	592	650	2.813	ZP
28120	NGC 2976	8.98	9.89	9.97	0.53	60.	129	149	2.173	ZP
28630	NGC 3031	5.20	6.29	6.28	0.54	59.	416	485	2.686	ZP
30197	NGC 3198	9.17	10.33	10.28	0.39	70.	296	315	2.498	ZP
30819	IC2574	10.12	11.12	11.16	0.40	69.	106	113	2.054	ZP
31671	NGC 3319	10.55	11.82	11.72	0.54	59.	195	227	2.356	ZP
32007	NGC 3351	8.33	9.20	9.31	0.70	47.	262	312	2.556	ZP
32192	NGC 3368	7.88	8.80	8.88	0.64	52.	329	418	2.621	ZP
34554	NGC 3621	8.01	9.01	9.05	0.45	66.	266	292	2.465	ZP
34695	NGC 3627	7.39	8.28	8.38	0.53	60.	333	385	2.585	ZP
39422	NGC 4244	8.92	10.25	10.12	0.20	90.	192	192	2.283	ZP
39600	NGC 4258	6.84	7.98	7.95	0.40	69.	414	444	2.647	ZP
40596	NGC 4395	9.08	11.21	10.66	0.73	44.	112	161	2.206	ZP
40692	NGC 4414	8.73	9.38	9.60	0.60	55.	378	463	2.666	ZP
41812	NGC 4535	8.95	9.75	9.89	0.72	45.	265	374	2.573	ZP
41823	NGC 4536	9.03	9.85	9.98	0.38	71.	322	341	2.533	ZP
42408	NGC 4605	9.19	10.17	10.22	0.41	69.	154	165	2.219	ZP
42510	NGC 4603	9.76	10.67	10.75	0.64	52.	353	450	2.653	ZP
42741	NGC 4639	10.18	11.27	11.26	0.60	55.	274	336	2.526	ZP
43451	NGC 4725	7.84	8.87	8.89	0.56	58.	397	470	2.672	ZP
47368	NGC 5204	/	11.93	/	0.50	62.	186	267	2.095	ZP
60921	NGC 6503	8.67	9.78	9.76	0.32	75.	223	231	2.363	ZP
69327	NGC 7331	7.52	8.39	8.50	0.44	66.	501	547	2.738	ZP
73049	NGC 7793	8.25	9.27	9.30	0.62	53.	162	202	2.306	ZP
...										

Table 2. Properties of the cluster fits: (1) cluster name, (2) mean velocity of the cluster with respect to the CMB corrected for cosmological effects, km s^{-1}, (3) error on the velocity, km s^{-1}, (4) number of studied galaxy per cluster for the original TFR and for the colour-corrected TFR, (5) slope of the inverse fit, (6) zero-point relative to Virgo's zero-point, no colour adjustment, mag, (7) scatter, no colour adjustment, (8) zero-point relative to Virgo's zero-point after colour adjustment, mag, (9) scatter after colour adjustment, mag, (10) bias, mag, (11) bias-corrected distance modulus, mag, (12) cluster distance, Mpc, (13) Hubble parameter, km s^{-1} Mpc^{-1}.

Cluster	$V_{\rm mod}$	eV	N	Slope	ZP	rms	$\rm ZP_{color}$	rms	bias	DM	Dist	V/D
V Virgo	1495	37	30–30	− 9.88 ± 0.73	10.50 ± 0.12	0.64	10.63 ± 0.10	0.55	0.00	30.94 ± 0.12	15.4 ± 0.9	97.0 ± 5.9
F Fornax	1358	45	15–15	− 9.56 ± 0.63	10.77 ± 0.12	0.46	10.85 ± 0.11	0.42	0.00	31.16 ± 0.13	17.1 ± 1.0	79.6 ± 5.4
U U Ma	1079	14	35–34	− 9.32 ± 0.52	10.74 ± 0.11	0.64	10.80 ± 0.10	0.57	0.00	31.11 ± 0.12	16.7 ± 0.9	64.7 ± 3.7
An Antlia	3198	74	18–13	− 10.07 ± 1.33	12.37 ± 0.12	0.52	12.48 ± 0.07	0.27	0.05	32.84 ± 0.10	37.0 ± 1.7	86.5 ± 4.5
Ce Cen30	3823	82	14–12	− 12.92 ± 1.74	12.51 ± 0.16	0.60	12.58 ± 0.16	0.55	0.00	32.89 ± 0.17	37.8 ± 3.0	101.0 ± 8.2
Pe Pegasus	3062	78	16–16	− 9.84 ± 1.03	12.91 ± 0.14	0.55	12.94 ± 0.11	0.44	0.01	33.26 ± 0.13	44.9 ± 2.7	68.2 ± 4.4
H Hydra	4088	72	25–19	− 9.12 ± 0.94	13.38 ± 0.14	0.71	13.52 ± 0.13	0.55	0.01	33.84 ± 0.14	58.6 ± 3.8	69.7 ± 4.7
Pi Pisces	4759	39	52–52	− 11.02 ± 0.75	13.77 ± 0.07	0.50	13.76 ± 0.06	0.45	0.03	34.10 ± 0.09	66.1 ± 2.7	72.0 ± 3.0
Ca Cancer	5059	82	12–12	− 11.65 ± 1.02	13.74 ± 0.11	0.39	13.75 ± 0.10	0.31	0.02	34.08 ± 0.11	65.5 ± 3.3	77.3 ± 4.1
Co Coma	7370	76	23–23	− 7.97 ± 0.67	14.42 ± 0.10	0.49	14.40 ± 0.09	0.42	0.07	34.78 ± 0.11	90.4 ± 4.6	81.6 ± 4.2
A4 A400	7228	97	7–7	− 8.00 ± 1.38	14.47 ± 0.11	0.48	14.46 ± 0.09	0.42	0.15	34.92 ± 0.12	96.4 ± 5.3	75.0 ± 4.3
A1 A1367	6969	93	20–20	− 9.32 ± 0.92	14.53 ± 0.08	0.21	14.53 ± 0.07	0.19	0.10	34.94 ± 0.10	97.3 ± 4.5	71.6 ± 3.4
A2 A2634/66	8938	164	20–20	− 9.55 ± 0.97	14.82 ± 0.11	0.50	14.88 ± 0.10	0.43	0.09	35.28 ± 0.12	113.8 ± 6.3	78.6 ± 4.6

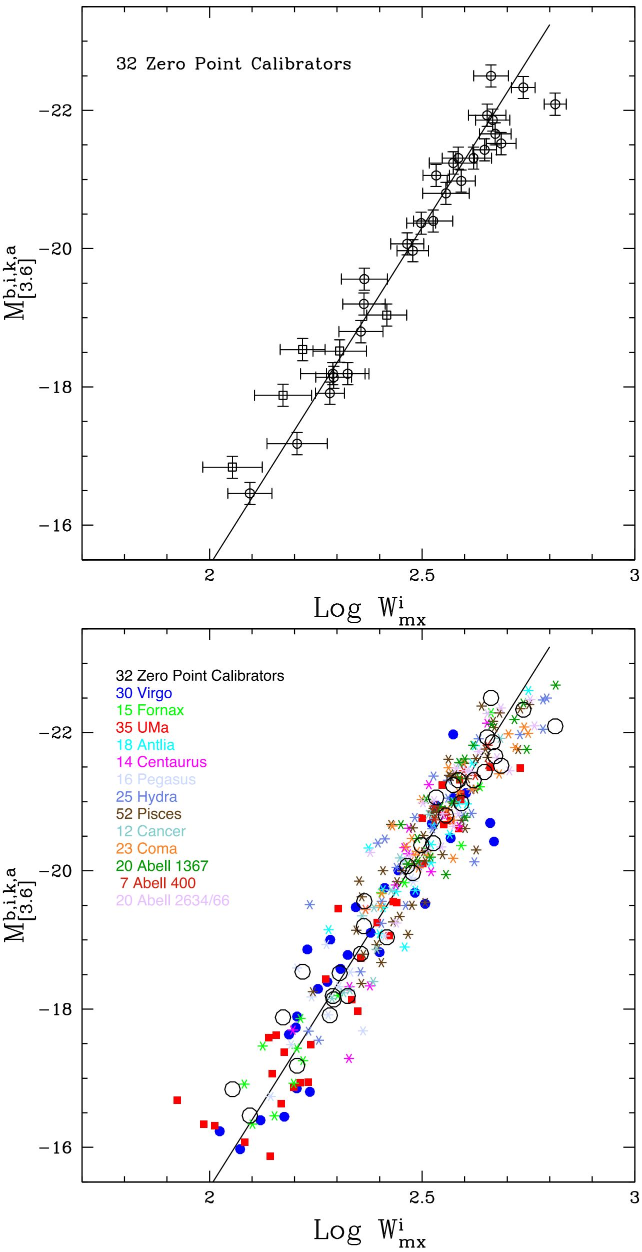

Figure 10. Top: inverse TFR for the 32 zero-point calibrators with distances obtained with Cepheids (circles) or Tip of the red giant branch (squares). The slope of the solid line is given by the luminosity–linewidth correlation of the template cluster while the zero-point is obtained with the least-squares fit to the 32 galaxies. The zero-point is set at $\log W^i_{mx} = 2.5$. Bottom: inverse TFR at 3.6 μm with the slope built out of 287 galaxies in 13 clusters and the zero-point set by 32 galaxies with very accurate distances.

The robustness of the procedure and of the derived TFR is confirmed. Namely, no major bias affects the relation as it is almost independent of the calibrator sample in terms of completeness and band selection.

4.3 Bias and distances

Although all TFRs (individual and universal) derived in this paper are inverse fits (errors solely in linewidths), a small Malmquist selection bias residual remains. This bias was investigated with the S13 TFR calibration at 3.6 μm. In this paper, the situation is

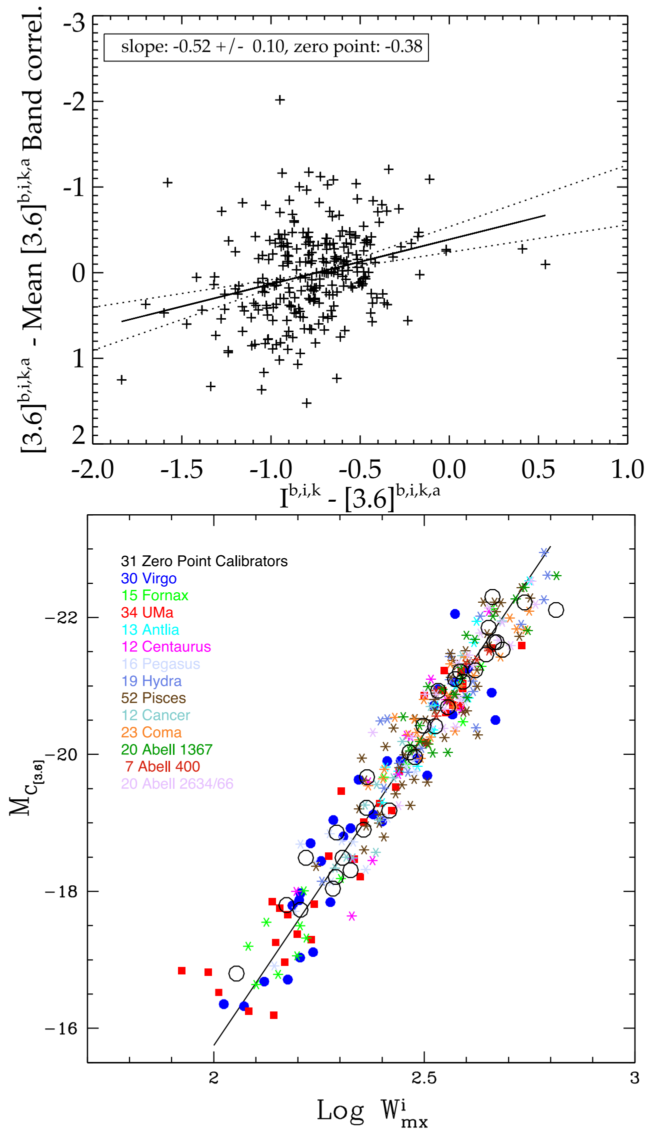

Figure 11. Top: deviation from the universal inverse TFR as a function of $I^{b,\,i,\,k} - [3.6]^{b,\,i,\,k,\,a}$ colour. The solid line stand for the best fit while the dotted lines represents the 95 per cent probability limits. Redder galaxies tend to lie above the relation while bluer galaxies are preferentially below the relation. Bottom: relation for pseudo-absolute magnitudes with the zero-point set by galaxies with independent very accurate distance estimates (open circles).

improved because galaxies are selected in *K* (instead of *B*) band. This change in wavelength selection reduces the interval between sample selection and photometry bands. However, because of the morphology of the luminosity function, galaxies are not scattered up and down exactly similarly. The amplitude of the bias increases with distance as the selection limit approaches the exponential cutoff of the luminosity function.

As a result, the same bias analysis as in S13 is conducted but without consideration of a faint end cutoff colour dependence. Virgo, Fornax and Ursa Major are modelled with a Schechter (1976) function with a faint end slope of −1.0 and a bright end cutoff at −22. Then, a random population is built out of this Schechter function to match the TFR at 3.6 μm in terms of slope, zero-point and scatter. The bias is estimated as the average deviation of sampled distances from the input TFR for successive brighter cutoffs with the

Table 3. TFR parameters in Courtois & Tully (2012b) for the *I* band obtained with the *B*-band-selected calibrator sample, in S13 for the 2013 [3.6] calibration derived with part of the *B*-band-selected calibrator sample and in this paper for the calibration computed with the *K*-band-selected calibrator sample.

Sample	N_{gal}	Slope	rms	Zero-point
I template	267	-8.81 ± 0.16	0.41	–
I zero-point	36	–	0.36	-21.39 ± 0.07 (Veg)
2013 [3.6] template	213	-9.74 ± 0.22	0.49	–
2013 [3.6] zero-point	26	–	0.44	-20.34 ± 0.10 (AB)
2013 M_C template	213	-9.13 ± 0.22	0.44	–
2013 M_C zero-point	26	–	0.37	-20.34 ± 0.08 (AB)
This paper [3.6] template	287	-9.77 ± 0.19	0.54	–
This paper [3.6] zero-point	32	–	0.45	-20.31 ± 0.09 (AB)
This paper M_C template	273	-9.10 ± 0.21	0.45	–
This paper M_C zero-point	31	–	0.37	-20.31 ± 0.07 (AB)

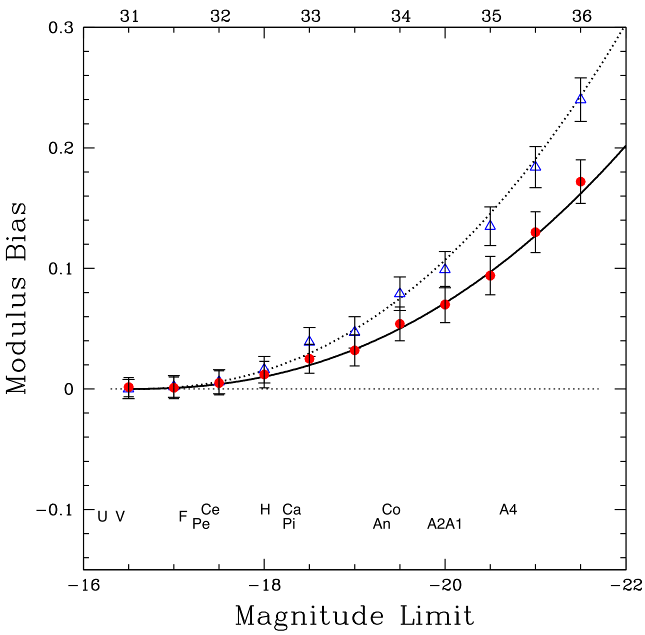

Figure 12. Bias measured as a function of absolute magnitude cutoff. The dotted and solid black curves are fits to the blue triangles and red filled circles which are bias estimates at successive cutoffs for the [3.6] TF calibration and for the colour adjusted TFR. The formula for the curves are $0.006(\mu - 31)^{2.3}$ and $0.004(\mu - 31)^{2.3}$. Letters at the bottom stand for the 13 clusters given in Table 2. They are positioned at the magnitude limits of clusters and their vertical projections on to the curve give the corresponding biases. The bias for an individual galaxy with a measured modulus is given by projection on to the curves from the top axis.

convention, bias = input TFR − measured TFR for the different cutoff samples. The corresponding curve normalized to zero at a distance modulus of 31 is shown in Fig. 12 and can be written as

$$\text{bias} = 0.004(\mu - 31)^{2.3}, \tag{4}$$

where μ is the distance modulus. The coefficient 0.004 is smaller than in S13 (0.0065) because of the previous colour dependence. However, the 2.3 exponent is larger than before because of a larger assumed scatter. The scatter dominates the bias relic. At the bottom of Fig. 12, letters standing for the 13 clusters are positioned at their cutoffs while the corresponding biases are given by projection on to the curve. Bias corrections for each cluster are given in Table 2 alongside the letters to match them with the names of clusters. Corrections are already included in moduli and distances given in this same table. As for an individual galaxy, the bias-corrected distance modulus μ is obtained by adding $0.004(\mu - 31)^{2.3}$. For completeness, the bias correction for the non-colour-adjusted relation, obtained similarly, is given by bias = $0.006(\mu - 31)^{2.3}$.

Distances obtained for the 13 clusters are compared with previous estimates (S13 and *I* band) in Table 4. Overall distances are in good agreement with each other and within uncertainties. Combining these distances with velocities with respect to the CMB corrected with a cosmological model assuming $\Omega_m = 0.27$ and $\Omega_\Lambda = 0.73$ (Tully et al. 2013), it is possible to derive a 'Hubble parameter' for each cluster. These values are given in Table 2 and plotted in Fig. 13. A straight line fit to the logarithms of these parameters for clusters at a distance greater than 50 Mpc gives a Hubble value of 75 ± 4 (ran) km s^{-1} Mpc^{-1} where (ran) stands for twice the 1σ random error.

5 CONFIRMING HUBBLE CONSTANT ESTIMATE WITH SUPERNOVAE

At the time of Sorce et al. (2012b) only 39 hosts of SNIa had been observed with *Spitzer*. Now, 45 host galaxies have all the required parameters to be compared with SNIa measurements. The new information extends the previous work by only six galaxies and we do not expect much change with regard to the offsets between SNIa and TF distance moduli estimates, nor [3.6] band measurements especially because the calibration at 3.6 μm has been shown to be very robust. Still, for the sake of completeness, raw magnitudes of these galaxies are corrected as before and the corresponding pseudo-magnitudes are derived. The colour-corrected TFR is applied to this set of supernova hosts to derive distance moduli estimates. These distance moduli are then bias corrected and compared with distance moduli obtained from supernova measurements to determine the supernova zero-point scale. All the parameters are gathered in Table 5. Fig. 14 shows the results when the six additional galaxies are included in the sample and the TFR is used to derive moduli. 8 of the 13 calibration clusters with observed SNIa are also added. The straight line is a fit, assuming slope unity, to the 45 individual galaxies each with weight 1 and six clusters each with weight 9 (Centaurus and Abell 1367 have been rejected in Sorce et al. (2012b) and distance moduli for Virgo and Fornax include contributions from Cepheid and Surface Brightness Fluctuation methods for consistency with the previous work). The offset is identical to that found in S13. Our Hubble constant estimate is unchanged $H_0 = 75.2 \pm 3.3$ km s^{-1} Mpc^{-1}.

Table 4. Comparison with S13 and Courtois & Tully (2012b): (1) cluster name, (2) this paper distance, Mpc, (3) S13 distance, Mpc (4) Courtois & Tully (2012b) distance, Mpc.

Cluster	This paper	2013 paper	TC12	Cluster	This paper	2013 paper	TC12
V Virgo	15.4 ± 0.9	14.7 ± 0.9	15.9 ± 0.8	Pi Pisces	66 ± 3	65 ± 3	64 ± 2
F Fornax	17.1 ± 1.0	17.4 ± 1.2	17.3 ± 1.0	Ca Cancer	66 ± 3	67 ± 4	65 ± 3
U U Ma	16.7 ± 0.9	18.0 ± 0.9	17.4 ± 0.9	Co Coma	90 ± 5	95 ± 6	90 ± 4
An Antlia	37 ± 2	37 ± 2	37 ± 2	A4 A400	96 ± 5	97 ± 5	94 ± 5
Ce Cen30	38 ± 3	39 ± 4	38 ± 3	A1 A1367	97 ± 5	96 ± 6	94 ± 5
Pe Pegasus	45 ± 3	45 ± 3	43 ± 3	A2 A2634/66	114 ± 6	112 ± 7	/
H Hydra	59 ± 4	56 ± 4	59 ± 4	A2634		/	121 ± 7

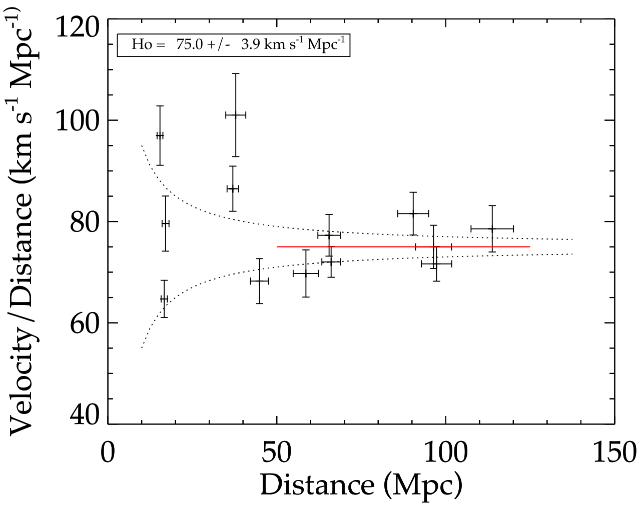

Figure 13. Hubble parameter as a function of distance. The solid red line at 75.0 ± 3.9 km s^{-1} Mpc^{-1} is a fit to the logarithms of cluster 'Hubble parameters' at distances greater than 50 Mpc. The dotted line represents the average 200 km s^{-1} deviation from the expansion due to peculiar motions.

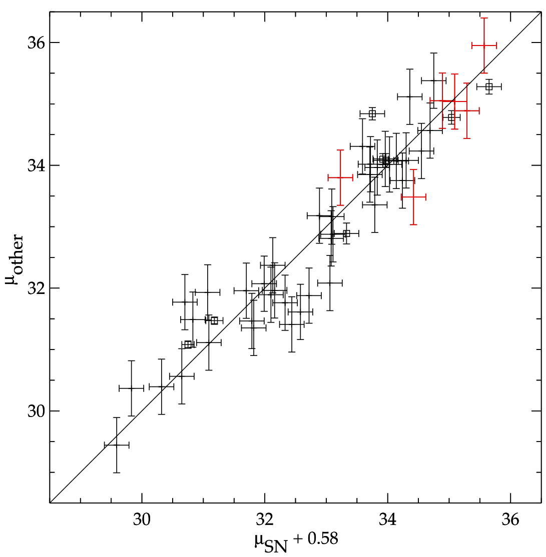

Figure 14. Top: comparison between moduli derived with SNIa and with 'other' methods (TFR, with Cepheid and surface brightness fluctuation supplements). The solid line has for slope the weighted fit to the 45 galaxies (filled points) with TFR distances and six of the eight clusters (open squares) and a null zero-point.

6 A CATALOGUE OF ACCURATE DISTANCE ESTIMATES

This paper has been the occasion to release the observational campaign CFS, a photometric component of the Cosmicflows project. The primarily goal of this observational survey is to increase the number of distance estimates close to the Zone of Avoidance using the TFR. The first channel (3.6 μm) of the IRAC on board the *Spitzer* Space Telescope is indeed the instrument of choice to obtain the required excellent photometry. At this wavelength the Zone of Avoidance and uncertainties on measurements are considerably reduced. Surface photometry of 1270 galaxies constituting the CFS sample observed in cycle 8 with IRAC channel 1 and over 400 additional galaxies observed in various other surveys have been presented in Sections 2 and 3. The S^{4}G supplies many more galaxies of interests to the Cosmicflows project.

The final set is constituted of 1935 galaxies with required parameters (in particular W_{mx}, b/a, [3.6] and if available I magnitudes), to derive an estimate of their distance with the mid-infrared (colour adjusted) TFR derived in Section 4, all available. Axial ratios come either from previous estimates of the Cosmicflows programme or from HyperLeda if they are from Paturel et al. (2003). I-band magnitudes come from a multitude of surveys set on the same scale. The compilation of I-band magnitudes is described in Tully et al. (2013). It gathers magnitudes used in Tully & Pierce (2000) and Tully et al. (2008), themselves borrowing from Giovanelli et al. (1997), Mathewson, Ford & Buchhorn (1992), Pierce & Tully (1988), Tully et al. (1996), but also recent derivations from Courtois, Tully & Héraudeau (2011b), Springob et al. (2007) and Hall et al. (2012). Tully et al. (2013) showed that these I-band magnitudes are on a consistent scale after small adjustments with the exception of those of Hall et al. (2012) because they use a significantly different filter. Accordingly, these later are corrected with the formulas prescribed by Smith et al. (2002) and Tully et al. (2013). These corrections involve a translation from Sloan g, r, i band (Gunn i band) to Cousins I band:

$$I^c_{\rm sdss} = i - 0.14(g - r) - 0.35, \quad (5)$$

where cases with $r - i \geq 0.95$ are excluded, and account for a slight tilt between $I^c_{\rm sdss}$ and I_c, from the Cosmicflows project, magnitudes,

$$I_c = 1.017\ I^c_{\rm sdss} - 0.221. \quad (6)$$

I-band magnitudes are extinction and k-corrected with the formulas given in Chilingarian, Melchior & Zolotukhin (2010), Tully & Pierce (2000). Then, I-band magnitudes are converted to the AB system. [3.6] magnitudes are also corrected and pseudo-magnitudes are derived. Combined with the (colour-corrected) TFR applied to linewidths, these latter enable the derivation of distance moduli. Distance moduli are corrected for the selection bias before deriving

Table 5. Properties of individual SNIa galaxies (latest results): (1) common name, (2) PGC name, (3) mean velocity of host galaxy with respect to the CMB, km s^{-1}, (4) mean velocity of host galaxy with respect to the CMB corrected for the cosmological model, km s^{-1}, (5) corrected rotation rate parameter corresponding to twice the maximum velocity, km s^{-1}, (6) corrected 3.6 μm magnitude in the AB system, mag, (7) colour-adjusted magnitude, mag, (8) absolute colour-adjusted magnitude, mag, (9) TFR distance modulus corrected for bias, mag, (10) SNIa distance modulus, mag. Supplementary galaxies with respect to the 2012 work are in red.

Name	PGC	$v_{\rm CMB}$	$v_{\rm mod}$	W^i_{mx}	$[3.6]^{b,i,k,a}$	$C_{[3.6]}$	$M_{C_{[3.6]}}$	$\mu_{\rm TF}$	$\mu_{\rm SN}$
UGC00139	963	3975	3626	311	13.43	13.51	−20.25	33.80	33.33
UGC00646	3773	5348	4898	389	12.85	12.84	−21.13	34.02	33.82
PGC005341	5341	1964	1601	236	12.84	12.72	−19.15	31.88	32.82
NGC 0673	6624	5241	5051	444	11.96	12.15	−21.66	33.85	33.81
NGC 0958	9560	5732	5623	592	11.09	11.23	−22.79	34.08	34.40
UGC01993	9618	8005	7967	485	12.97	12.94	−22.00	35.04	35.19
IC1844	10448	6846	6693	309	13.55	13.23	−20.22	33.48	34.52
ESO300-009	11606	6045	6017	321	14.67	14.64	−20.37	35.12	34.46
PGC011767	11767	8701	8671	422	13.16	13.35	−21.46	34.89	35.39
NGC 1448	13727	1194	1062	388	9.97	9.99	−21.12	31.11	31.19
UGC03329	17509	5253	5668	524	11.74	11.65	−22.31	34.01	34.13
UGC03375	18089	5783	5879	534	11.63	11.67	−22.38	34.10	34.06
PGC018373	18373	2168	2281	239	12.45	12.54	−19.22	31.76	32.43
UGC03432	18747	4996	5080	289	13.93	13.96	−19.96	33.96	33.93
UGC03576	19788	5966	6009	392	12.94	13.01	−21.17	34.23	34.65
UGC03770	20513	6378	6646	371	13.48	13.55	−20.95	34.57	34.79
UGC03845	21020	3034	3166	257	13.33	13.36	−19.50	32.88	33.21
NGC 2841	26512	637	810	650	8.63	8.61	−23.16	31.77	30.80
NGC 3021	28357	1515	1781	302	11.64	11.82	−20.14	31.96	32.26
NGC 3294	31428	1567	1838	431	10.76	10.82	−21.54	32.37	32.23
NGC 3368	32192	906	1332	427	8.77	8.86	−21.50	30.37	29.93
NGC 3370	32207	1367	1622	311	11.69	11.81	−20.26	32.07	32.09
NGC 3627	34695	723	1454	384	8.26	8.36	−21.08	29.44	29.69
NGC 3663	35006	5040	5389	443	12.42	12.37	−21.65	34.07	34.24
NGC 3672	35088	1860	2210	399	10.57	10.66	−21.23	31.89	32.20
NGC 4501	41517	2268	1740	570	8.75	8.85	−22.64	31.49	30.93
NGC 4527	41789	1736	2090	361	9.32	9.56	−20.84	30.39	30.42
NGC 4536	41823	1808	2162	341	9.81	9.95	−20.61	30.56	30.75
NGC 4639	42741	1003	1740	348	11.25	11.26	−20.69	31.96	31.80
NGC 4680	43118	2491	2811	237	12.10	12.24	−19.17	31.41	32.54
NGC 4679	43170	4665	3824	426	11.72	11.84	−21.49	33.36	33.89
NGC 5005	45749	1011	1177	601	9.01	9.08	−22.85	31.93	31.17
ESO576-040	46574	2095	2407	169	13.72	13.61	−17.85	31.47	31.89
PGC047514	47514	4217	4577	284	13.96	13.82	−19.89	33.75	34.34
NGC 5584	51344	1655	191	266	11.74	11.72	−19.64	31.35	31.92
IC4423	51549	9115	9691	470	13.73	13.92	−21.88	35.95	35.67
IC1151	56537	2176	2287	241	12.83	12.83	−19.25	32.08	33.16
NGC 6063	57205	2841	2958	308	12.98	12.95	−20.21	33.18	32.99
UGC10738	59769	6716	6850	584	12.37	12.53	−22.74	35.38	34.85
UGC10743	59782	2744	2581	218	12.59	12.76	−18.85	31.61	32.68
NGC 6962	65375	4200	3695	639	11.05	11.15	−23.09	34.31	33.69
IC5179	68455	3400	3108	444	10.80	11.14	−21.66	32.81	33.18
UGC12133	69428	7391	7213	442	13.17	13.32	−21.64	35.05	34.99
NGC 7329	69453	3245	3150	461	11.19	11.34	−21.80	33.16	33.19
NGC 7448	70213	2170	1752	309	11.32	11.40	−20.23	31.63	32.72

distance estimates. Table 6 (complete table online) gives the first few derived distance estimates. Eventually these distance estimates will be incorporated into a new data release of the Cosmicflows project, increasing the size of the previous catalog by 20 per cent, including spatial regions close to the Zone of Avoidance.

7 CONCLUSION

With the new generation of sensitive telescopes/detectors both in the radio band and in the photometric domain, cosmic flow studies have received an impetus. The space-based *Spitzer* telescope is an example of such a telescope with enhanced capacities. With a *Spitzer*-adapted version of the software ARCHANGEL, we have obtained surface brightness photometry and distances for 1270 galaxies that are part of the CFS programme, itself included in the larger *Cosmicflows* project. An increase in the number of TF calibrators since the 2013 calibration and a superior selection criteria using the *K*-band instead of *B* band led us to recalibrate the 3.6 μm TFR. The derived relation confirms the robustness of the 2013 calibration and is given by $M_{C_{[3.6]}} = -(20.31 \pm 0.07) - (9.10 \pm$

Table 6. Distance measurements for 1935 galaxies observed with *Spitzer* for which we have all the parameters requested (in particular W_{mx}, b/a, [3.6] and, for 1511 galaxies, I) to compute an estimate (complete table online): (1) Principal Galaxy Catalog number, (2) common name, (3) Rad and Dec., J2000 system, (4) galactic longitude, degrees, (5) galactic latitude, degrees, (6) supergalactic longitude, degrees, (7) supergalactic latitude, degrees, (8) heliocentric velocities, km s^{-1}, (9) velocity with respect to the cosmic microwave background modified for the cosmology, km s^{-1}, (10) numerical morphological type, (11) axial ratio, (12) H I linewidth, km s^{-1}, (13) logarithm of the de-projected H I linewidth, km s^{-1}, (14) I-band magnitude, mag (Vega system), (15) I-band magnitude corrected for extinctions and k-corrected, mag (AB system), (16) [3.6]-band magnitude, mag (AB system), (17) extinctions, aperture and k-corrected [3.6]-band magnitude, mag (AB system), (18) pseudo apparent magnitude at [3.6], mag, (19) pseudo absolute magnitude at [3.6], mag, (20) apparent magnitude at [3.6], mag, (21) absolute magnitude at [3.6], mag, (22) distance modulus corrected for the selection bias obtained with the colour-adjusted TFR, mag, (23) selection-bias-corrected distance estimates obtained with the colour-adjusted TFR, Mpc, (24) distance modulus corrected for the selection bias obtained with the TFR, mag, (25) selection-bias-corrected distance estimates obtained with the TFR, Mpc.

PGC	Name	Ra-Dec J2000	l	b	sgl	sgb	v_h	$v_{\rm mod}$	t	b/a	w_{mx}	$\log w^i_{mx}$	I	$I^{b,i,k}$	[3.6]	$[3.6]^{b,i,k,a}$	$C_{[3.6]}$	M_C	$M_{[3.6]}$	μ_C	d_C	$\mu_{[3.6]}$	$d_{[3.6]}$
218	NGC 07814	J000314.9+160844	106.4089	−45.1745	309.0614	16.4026	1051	695	2.0	0.20	455	2.658	9.18	8.63	9.61	9.57	9.46	−21.75	−21.85	31.20	17.4	31.42	19.2
255	UGC00017	J000343.2+151305	106.2149	−46.0989	308.1422	16.0958	878	521	9.1	0.63	98	2.092	13.85	14.07	14.78	14.87	14.83	−16.60	−16.33	31.43	19.3	31.20	17.4
279	NGC 007817	J000358.9+204508	108.2283	−40.7605	313.8141	17.1420	2311	1970	4.1	0.26	411	2.620	10.62	10.22	10.84	10.87	10.91	−21.40	−21.48	32.31	29.0	32.36	29.7
527	UGC000054	J000653.8+414426	114.0896	−20.3652	335.8192	19.2667	4249	3993	6.0	0.20	192	2.283	/	/	15.96	16.04	/	/	−18.19	/	/	34.32	73.1
627	AGC020097	J000820.9-295455	13.9928	−80.1378	264.5900	1.9316	1497	1214	4.8	0.21	158	2.200	12.91	12.94	13.92	14.00	13.82	−17.58	−17.37	31.40	19.0	31.38	18.8
698	NGC 00023	J000953.4+255526	111.3675	−36.0132	319.3855	16.7229	4568	4275	1.2	0.68	367	2.692	10.83	10.90	11.20	11.31	11.47	−22.06	−22.19	33.56	51.6	33.54	51.1
701	AGC020114	J000956.3-245750	43.6860	−80.4343	269.3872	3.2262	554	250	5.1	0.30	202	2.317	10.40	10.38	11.43	11.44	11.27	−18.64	−18.52	29.91	9.6	29.96	9.8
767	NGC 00021	J001046.9+332110	113.2524	−28.7536	327.1050	17.6437	4770	4500	4.0	0.47	382	2.627	12.27	12.17	12.78	12.86	12.88	−21.47	−21.55	34.41	76.3	34.52	80.2
924	UGC00132	J001400.7+125750	108.9883	−48.8920	306.4453	13.1609	1696	1345	7.9	0.32	140	2.161	/	/	14.48	14.56	/	/	−17.00	/	/	31.56	20.5
963	UGC00139	J001431.9-004416	102.8519	−62.1619	292.9641	9.5361	3971	3652	5.1	0.43	287	2.493	12.89	12.83	13.44	13.52	13.54	−20.25	−20.25	33.83	58.3	33.83	58.4
1315	UGC00196	J002034.2+472603	117.5333	−15.1136	341.9918	17.2721	5150	4942	5.3	0.65	256	2.519	/	/	13.09	13.19	/	/	−20.49	/	/	33.74	56.0
1525	UGC00231	J002402.8+162911	113.4792	−45.8820	310.5250	11.6066	843	495	5.9	0.20	204	2.310	12.19	12.02	12.90	12.95	12.84	−18.58	−18.45	31.42	19.2	31.40	19.1
1651	AGC020302	J002646.4-334037	340.4905	−81.5678	262.2390	−2.9613	1831	1572	3.9	0.35	207	2.335	12.58	12.60	13.65	13.73	13.52	−18.81	−18.70	32.34	29.4	32.45	30.9
1658	UGC000256	J002656.5+500151	118.9045	−12.6493	344.7872	16.4431	5173	4978	4.0	0.20	331	2.520	13.02	12.45	12.70	12.74	12.96	−20.49	−20.50	33.49	49.8	33.28	45.3
1665	UGC00260	J002702.9+113502	113.4479	−50.8383	305.8528	9.7393	2134	1792	5.8	0.23	254	2.408	12.35	12.09	12.67	12.71	12.76	−19.47	−19.41	32.24	28.0	32.13	26.7
1713	UGC00272	J002749.7-011200	109.6294	−63.4603	293.4407	6.2135	3917	3604	6.4	0.40	236	2.402	13.58	13.58	14.65	14.74	14.51	−19.42	−19.35	33.98	62.5	34.17	68.4
1851	NGC 000134	J003021.9-331438	338.3093	−82.3778	262.8701	−3.5542	1583	1322	4.0	0.28	455	2.666	9.20	8.85	9.29	9.32	9.45	−21.82	−21.93	31.27	18.0	31.26	17.9
1921	UGC00312	J003123.9+082800	114.4661	−54.0753	303.0705	7.9214	4371	4065	8.0	0.42	285	2.488	12.71	12.65	13.44	13.53	13.45	−20.20	−20.19	33.69	54.6	33.78	57.1
1970	UGC00320	J003230.8+023427	113.4616	−59.9491	297.4139	6.1096	2394	2058	6.1	0.20	149	2.173	14.77	14.81	15.85	15.94	15.72	−17.34	−17.12	33.08	41.3	33.08	41.4
1977	IC0001553	J003240.1-253627	51.7638	−85.5297	270.3423	−1.8628	2929	2655	7.0	0.22	256	2.410	12.82	12.63	12.87	12.93	13.15	−19.49	−19.43	32.65	33.9	32.38	29.9
2052	AGC020385	J003415.5-274813	21.8940	−86.1300	268.3344	−2.8241	1580	1301	3.4	0.47	317	2.548	10.43	10.42	10.82	10.89	11.02	−20.74	−20.78	31.77	22.6	31.67	21.6
2071	IC0001555	J003432.7-300104	354.0143	−85.2990	266.2225	−3.5025	1530	1258	7.0	0.57	115	2.137	13.16	13.40	14.34	14.44	14.27	−17.01	−16.76	31.28	18.0	31.20	17.4
2142	IC0001558	J003546.6-252227	58.6007	−86.0752	270.7645	−2.4699	1551	1264	9.0	0.52	110	2.103	12.01	12.25	13.24	13.34	13.15	−16.69	−16.43	29.84	9.3	29.77	9.0
2437	AGC400333	J004035.0-135222	111.5732	−76.5046	282.1291	−0.3496	1638	1322	3.1	0.61	273	2.528	9.99	10.09	10.69	10.78	10.79	−20.57	−20.59	31.36	18.7	31.37	18.8
2445	ES079-005	J004044.2-632627	304.9496	−53.6455	233.6427	−12.4376	1712	1607	7.0	0.41	148	2.202	12.72	12.86	13.77	13.86	13.71	−17.60	−17.40	31.32	18.3	31.26	17.9
2479	UGC00438	J004127.9+252959	120.1021	−37.3172	320.3882	9.6661	4555	4276	5.0	0.70	346	2.675	11.13	11.23	11.63	11.74	11.85	−21.90	−22.02	33.79	57.4	33.82	58.1
2492	PG0002492	J004145.5-165142	110.1297	−79.4921	279.3344	−1.4478	1552	1243	2.0	0.68	134	2.253	/	/	14.05	14.15	/	/	−17.90	/	/	32.06	25.8
2526	AGC020471	J004214.7-180942	109.1648	−80.7868	278.1159	−1.9168	1554	1249	6.0	0.20	187	2.272	13.06	12.99	14.45	14.52	14.09	−18.23	−18.08	32.34	29.3	32.62	33.4
2699	UGC00477	J004613.1+192924	121.2400	−43.3647	314.7419	7.1900	2650	2331	7.9	0.20	223	2.348	13.20	13.01	14.23	14.29	14.00	−18.93	−18.83	32.95	38.9	33.15	42.7
2747	UGC00485	J004708.3+302028	121.8318	−32.5215	325.4576	9.5158	5248	4999	6.1	0.20	344	2.537	13.04	12.59	13.18	13.23	13.27	−20.64	−20.67	33.96	62.0	33.96	62.1
...																							

0.21)($\log W^i_{mx} - 2.5$) with a scatter of 0.43 mag (∼22 per cent in distance). $M_{C_{[3.6]}}$ is the pseudo-magnitude obtained after correction of [3.6] magnitudes by I−[3.6] colours, $M_{C_{[3.6]}} = M^{b,i,k,a}_{[3.6]} + (0.52 \pm 0.10)[(I^{b,i,k} - [3.6]^{b,i,k,a}) + 0.73]$, where I-band magnitude have been shifted to the AB system. Resulting distance moduli μ are then corrected for a tiny bias effect with the addition of the term $0.004(\mu - 31)^{2.3}$. Applying this calibration to a set of supernova hosts to obtain a scale for the supernovae, we confirm our Hubble constant estimate 75.2 ± 3.3 km s^{-1} Mpc^{-1}.

Drawing from the Spitzer archive, consistent magnitudes are available for 1935 galaxies that also have suitable H I linewidth measurements and appropriate morphologies and inclinations for the determination of TFR distances. This new material substantially augments the compilation of distances and derivative peculiar velocities in the *Cosmicflows* programme. The all-sky uniformity of the satellite photometry mitigates concerns that spatially correlated errors might induce artificial flows and the observations in the mid-infrared negate concerns with reddening even at low galactic latitudes. A parallel programme using mid-infrared data from the *WISE* complements the present study (Neill et al. 2014). Together, the new distances will make a major contribution to what will become Cosmicflows-3 and further enable reconstructions of local structure (Tully et al. 2014) and constrained simulations of the development of that structure (Sorce et al. 2014).

ACKNOWLEDGEMENTS

The data used in this paper are available at the EDD. We especially thanks our CFS collaborators Wendy Freedman, Barry Madore, Eric Persson and Mark Seibert. We are indebted to James Schombert for the development of the ARCHANGEL software and we thank him for his useful comments as a referee. We thank Kartik Sheth for discussions regarding *Spitzer* photometry. NASA through the Spitzer Science Center provides support for CFS, *Cosmicflows with Spitzer*, cycle 8 programme 80072. This research has made use of the NASA/IPAC Extragalactic Database (NED) which is operated by the Jet Propulsion Laboratory, California Institute of Technology, under contract with the National Aeronautics and Space Administration. We acknowledge the usage of the HyperLeda data base (http://leda.univ-lyon1.fr). HC and JS acknowledge support from the Lyon Institute of Origins under grant ANR-10-LABX-66 and from CNRS under PICS-06233. RBT acknowledges support from the US National Science Foundation award AST09-08846. TJ acknowledges the Astronomy Department of the University of Cape Town.

REFERENCES

Cardelli J. A., Clayton G. C., Mathis J. S., 1989, ApJ, 345, 245
Chilingarian I. V., Melchior A.-L., Zolotukhin I. Y., 2010, MNRAS, 405, 1409
Courtois H. M., Tully R. B., 2012a, Astron. Nachr., 333, 436
Courtois H. M., Tully R. B., 2012b, ApJ, 749, 174
Courtois H. M., Tully R. B., Fisher J. R., Bonhomme N., Zavodny M., Barnes A., 2009, AJ, 138, 1938
Courtois H. M., Tully R. B., Makarov D. I., Mitronova S., Koribalski B., Karachentsev I. D., Fisher J. R., 2011a, MNRAS, 414, 2005
Courtois H. M., Tully R. B., Héraudeau P., 2011b, MNRAS, 415, 1935
Dale D. A. et al., 2009, ApJ, 703, 517
de Vaucouleurs G., 1953, AJ, 58, 30
Erdoğdu P. et al., 2006, MNRAS, 373, 45
Fazio G. G. et al., 2004, ApJS, 154, 10
Fixsen D. J., Cheng E. S., Gales J. M., Mather J. C., Shafer R. A., Wright E. L., 1996, ApJ, 473, 576
Freedman W. L. et al., 2011, AJ, 142, 192
Giovanelli R., Haynes M. P., Salzer J. J., Wegner G., da Costa L. N., Freudling W., 1995, AJ, 110, 1059
Giovanelli R., Haynes M. P., Herter T., Vogt N. P., Wegner G., Salzer J. J., da Costa L. N., Freudling W., 1997, AJ, 113, 22
Hall M., Courteau S., Dutton A. A., McDonald M., Zhu Y., 2012, MNRAS, 425, 2741
Huang J.-S. et al., 2007, ApJ, 664, 840
Huchra J. P. et al., 2012, ApJS, 199, 26
Karachentsev I. D., Karachentseva V. E., Kudrya Y. N., Sharina M. E., Parnovskij S. L., 1999, Bull. Spec. Astrophys. Obser., 47, 5
Mathewson D. S., Ford V. L., Buchhorn M., 1992, ApJS, 81, 413
Monson A. J., Freedman W. L., Madore B. F., Persson S. E., Scowcroft V., Seibert M., Rigby J. R., 2012, ApJ, 759, 146
Muñoz-Mateos J. C. et al., 2009, ApJ, 703, 1569
Neill D. J., Seibert M., Tully R. B., Courtois H. M., Sorce J. G., Jarrett T., Scowcroft V., Masci F., 2014, ApJ, in press
Oke J. B., Sandage A., 1968, ApJ, 154, 21
Paturel G., Petit C., Prugniel P., Theureau G., Rousseau J., Brouty M., Dubois P., Cambrésy L., 2003, A&A, 412, 45
Pierce M. J., Tully R. B., 1988, ApJ, 330, 579
Reach W. T. et al., 2005, PASP, 117, 978
Riess A. G. et al., 2011, ApJ, 730, 119
Saunders W. et al., 2000, MNRAS, 317, 55
Schechter P., 1976, ApJ, 203, 297
Schlegel D. J., Finkbeiner D. P., Davis M., 1998, ApJ, 500, 525
Schombert J., 2007, preprint (arXiv:e-prints)
Schombert J., Smith A., 2012, Publ. Astron. Soc. Aust., 29, 174
Sheth K. et al., 2010, PASP, 122, 1397
Smith J. A. et al., 2002, AJ, 123, 2121
Sorce J. G., Courtois H. M., Tully R. B., 2012a, AJ, 144, 133
Sorce J. G., Tully R. B., Courtois H. M., 2012b, ApJ, 758, L12
Sorce J. G. et al., 2013, ApJ, 765, 94 (S13)
Sorce J. G., Courtois H. M., Gottlöber S., Hoffman Y., Tully R. B., 2014, MNRAS, 437, 3586
Springob C. M., Masters K. L., Haynes M. P., Giovanelli R., Marinoni C., 2007, ApJS, 172, 599
Tully R. B., Courtois H. M., 2012, ApJ, 749, 78
Tully R. B., Fisher J. R., 1977, A&A, 54, 661
Tully R. B., Pierce M. J., 2000, ApJ, 533, 744
Tully R. B., Verheijen M. A. W., Pierce M. J., Huang J.-S., Wainscoat R. J., 1996, AJ, 112, 2471
Tully R. B., Pierce M. J., Huang J.-S., Saunders W., Verheijen M. A. W., Witchalls P. L., 1998, AJ, 115, 2264
Tully R. B., Shaya E. J., Karachentsev I. D., Courtois H. M., Kocevski D. D., Rizzi L., Peel A., 2008, ApJ, 676, 184
Tully R. B., Rizzi L., Shaya E. J., Courtois H. M., Makarov D. I., Jacobs B. A., 2009, AJ, 138, 323
Tully R. B. et al., 2013, AJ, 146, 86
Tully R. B., Courtois H. M., Hoffman Y., Pomarède D., 2014, Nature, in press
Werner M. W. et al., 2004, ApJS, 154, 1
Wright E. L. et al., 2010, AJ, 140, 1868

SUPPORTING INFORMATION

Additional Supporting Information may be found in the online version of this article:

Table 1. Calibrator parameters for the TFR.

Table 6. Distance measurements for 1935 galaxies observed with *Spitzer* for which we have all the parameters requested (in particular W_{mx}, b/a, [3.6] and, for 1511 galaxies, I) to compute an estimate (http://mnras.oxfordjournals.org/lookup/suppl/doi:10.1093/mnras/stu1450/-/DC1).

Please note: Oxford University Press are not responsible for the content or functionality of any supporting materials supplied by the authors. Any queries (other than missing material) should be directed to the corresponding author for the paper.

This paper has been typeset from a TEX/LATEX file prepared by the author.